Both Ta and Nb under passive conditions did not absorb hydrogen. This result indicates that the passive films in HBr solutions are compact enough to avoid hydrogen permeation.

In the previous paper,[5] the authors concluded that both Ta and Nb were passivated in HBr solutions, judging from their electrochemical behavior and thermodynamic examinations on the stability of Ta_2O_5 and Nb_2O_5 in HBr solutions. Evaluation of corrosion resistance without information on their surface states and hydrogen absorption led us to an incorrect conclusion for Nb. At present, it can be said that Nb in HBr solutions free from oxidizing agents at high temperatures is not in a passivated state but in an active state.

CONCLUSIONS

▶ It has been reconfirmed that Ta is passivated in HBr solutions up to the azeotropic concentration of 47 wt% and to temperatures as high as 100°C. The passive film consisting of Ta_2O_5 can grow in HBr solutions. The film is stable enough to protect Ta from corroding and hydride formation.

▶ Nb is corrosion-resistant to HBr solutions at 25°C.

▶ Nb exhibits active and passive behavior, dependent on the condition of the HBr solution at high temperatures. In solution of a reducing condition, the growth of the protective oxide film does not proceed. Fine pits are formed initially and extend to general corrosion accompanied by hydrogen absorption. However, in the presence of an oxidizing agent, Nb is passivated, and the passive film consisting of Nb_2O_5 can grow.

▶ The stronger passivating tendency of both Ta and Nb in HBr solutions containing bromine than in HBr solutions bubbled with hydrogen is responsible for the difference in the rest potentials. The corrosion resistance of both metals is enhanced by shifting the electrode potential to the noble side. Although Nb is attacked by HBr solutions at high temperatures, the addition of oxidizing agents such as bromine to HBr solutions is effective in preventing Nb from corroding and from hydride formation.

REFERENCES

1. C.R. Bishop, M. Stern, Corrosion 17,8(1961): p. 379t.
2. D.L. MacLeary, Corrosion 18,2(1962): p. 67t.
3. Corrosion Data Survey-Metals Section (Houston, TX: National Association of Corrosion Engineers, 1977).
4. H.V.K. Udupa, V.K. Venkatesan, Encyclopedia of Electrochemistry of the Elements, vol. 2, ed. A.J. Bard (New York, NY: Marcel Dekker, Inc., 1974), p. 53.
5. I. Uehara, T. Sakai, H. Ishikawa, E. Ishii, M. Nakane, Corrosion 42,8(1986): p. 492.
6. G.G. Wuster, G. Wozny, Z. Giazitzoglou, Fluid Phase Equilibria 6(1981): p.93.
7. S. Matsuda, K. Sugimoto, J. Japan Inst. Metals 45,2(1981): p. 203.
8. S. Matsuda, K. Sugimoto, J. Japan Inst. Metals 49,3(1985): p. 224.
9. J.M. Sanz, S. Hofmann, J. Less-Common Metals 92(1983): p. 317.
10. J.S. Hammond, N. Winograd, Comprehensive Treatise of Electrochemistry, vol. 8 (New York, NY: Plenum Publ. Corp., 1984), p. 445.
11. C.P. Hunt, M.P. Seah, Surf. Interface Anal. 5,5(1983): p. 119.
12. C.D. Wagner, W.M. Riggs, L.E. Davis, J.F. Moulder, G.E. Muilenberg, Handbook of X-ray Photoelectron Spectroscopy, Perkin Elmer Corp., 1979.
13. P.C. Karulkar, J.E. Nordman, J. Vac. Sci. Technol. 11,1(1980): p. 462.
14. "JCPDS cards," no. 35-789 and no. 7-263.
15. T. Hurlen, H. Bentzen, S.Holnkjol, Electrochimica Acta 32,11(1987): p. 1613.
16. W. Wilhelmsen, Electrochimica Acta 33,1(1988): p. 63.

Electrochemical Potential Monitoring of Corrosion and Coating Protection of Mild Steel Reinforcement in Concrete ☆

*C.A. Loto and E.T. Odumbo**

ABSTRACT

The corrosion and protection behavior of a mild steel reinforcement in concrete, partially immersed in different test media, was investigated at ambient temperature by potential monitoring technique. The work was carried out using a digital voltmeter and a copper sulfate electrode (CSE) as the reference electrode. The obtained results showed that corrosion occurred on the embedded steel by the processes of anodic and cathodic reactions. The active corrosion of the steel occurred by the depassivation of the hydroxyl ions stablized passive film on the steel's surface and the consequent anodic dissolution of the reinforcement bars. The corrosion of the embedded steel was enhanced by the diffusion of chloride, sulfate, and carbonate ions from the test media, in addition to the absorbed oxygen and water/moisture. The coating of the reinforcement steel with paint before embedding in concrete block gave some measure of protection. Coating of the concrete blocks externally was a more protective method. However, a combination of the steel coating and external coating of the concrete block showed the most effective corrosion protection comparatively.

KEY WORDS: concrete, coatings, electrochemical, potential, protection, reinforcement

INTRODUCTION

Concrete is a complex material of construction that enables the

☆ Submitted for publication December 1987, revised June 1988.

* Department of Metallurgical and Materials Engineering, Obafemi Awolowo

configuration.[1] Reinforced concrete is a widely accepted material of construction. It has functioned more or less acceptably in many environments, and while some deterioration of reinforcing steel has been noted, the problems have been so far outweighed by the good experiences.[2] While various other research works on different aspects of this subject have been reported by a number of investigators,[3-12] many features are not yet clearly defined. In fact, most of the research work has been mainly concentrated in the temperate countries, while reports in the tropical areas are almost nonexistent.

Damage to structures such as spalling, cracking and sometimes collapse of buildings and bridges has been observed. There has also been increasing deterioration of marine reinforced concrete structures. This investigation has been carried out by the potential monitoring of the corrosion behavior of a locally produced mild steel reinforcement in concrete, with the aim of gaining more insight in this corrosion mechanism. The study also looks at the paint coating of the reinforcement steel and the concrete blocks externally as a protective measure for the reinforced concrete structures particularly in the tropical areas. Painting of buildings is continually being done, for example, in Nigeria for an aesthetic purpose only. The various test media used thus simulate different environments in which steel-reinforced concrete structures are being used, including the industrial atmospheric environments.

EXPERIMENTAL PROCEDURE

Preparation of Concrete Block Samples

Concrete blocks made of portland cement, gravel, sand, and water, each one with a reinforcing steel bar embedded in it, were cast. Each block was 160-mm long, 100-mm wide, and 100-mm thick. The concrete blocks were allowed to set and hardened for 3 days before being used for experiments.

Some concrete blocks were cast with some quantities of NaCl (AnalaR grade). The amount of salt added was dissolved in de-ionized water with which the concrete mix was made to ensure uniform introduction of the chloride ions into the blocks.

Four other different categories of concrete block were cast:

- those without NaCl content,
- those without NaCl content and with painted steel bar embedded in them,
- those without NaCl and the blocks painted externally, and
- those without NaCl but with painted embedded steel bar and the blocks painted externally.

In each case of paint coating, ICI[1] zinc-rich epoxy paint was used and three coats of paint applied.

The cement:sand:gravel (C:S:G) ratio of 1:2:4 was the same for all the concrete blocks used in this work. All the steel bars used for reinforcement were cut out from the same stock. The steel was of DIN[2] ST-60-Mn from Oshogbo Steel Rolling Mill[3] with the chemical composition of 0.3% C, 0.25% Si, 1.5% Mn, 0.04% P, 0.64% S, 0.25% Cu, 0.1% Cr, 0.11% Ni, and the rest, Fe. Each one had the same dimensions, with a length of 160 mm and a diameter of 14 mm. An abrasive grinder was used to remove any mill scale and rust stains on the steel specimens before being embedded in the concrete block during casting. Each steel rod was symmetrically placed across the width of the block in which it was embedded. Only about 140 mm of each steel bar of length 160 mm was embedded in each concrete block. The remaining 20 mm (used for electrical connection) protruded at one end of the concrete (Figure 1).

Test Media

The test media used in this investigation were 0.2 M $NaHCO_3$ solution, 1 M NaCl solution, seawater, and tap water.

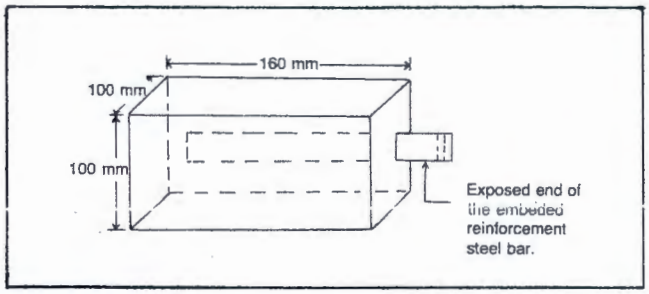

FIGURE 1. *A sample block (not to scale).*

Potential Measurements

The experimental set up for potential measurements is as shown in Figure 2. The experiment was conducted with each concrete block partially immersed in its respective test media. Readings were taken on each of the partially immersed blocks. A constant distance of 1 cm from the steel bar was kept from the medium surface to ensure the solution did not make contact with the exposed part of the steel bar. The exposed part of the steel was coated with paint except for a hole that was drilled at this end for electrical connection.

Readings were obtained by separately placing a block from each of the categories previously mentioned, in turns, in a vessel containing the prepared test solution. A copper sulfate electrode was then clamped firmly on the concrete block and the electrical connecting circuit was completed as shown in Figure 2. Readings were taken at three different points on each block. The initial voltage readings were taken for each block and subsequent readings were then taken at regular 5-day intervals. The copper sulfate electrode was placed on the block so that it was directly over the embedded steel bar. All the experiments were carried out under free corrosion potentials at ambient temperature.

RESULTS AND DISCUSSION

Steel Reinforcement in Concrete with Premixed NaCl—Environmental Effects

Figure 3 shows the curves of the corrosion potential vs the exposure time (days) for the steel-reinforced concrete blocks, with NaCl content, partially immersed in seawater, 0.2 M $NaHCO_3$ solution, 1 M NaCl solution, and in tap water. From the curves, a trend of increasing, though fluctuating, negative potentials could be observed throughout the experimental period. This is an indication of active corrosion. The increasing negative potentials with time must have been caused by anodic dissolution of the embedded steel surface. The effect then might be the occurrence of localized corrosion in the form of pitting and/or general corrosion. As shown in Figure 3, the observed active corrosion phenomenon might have been caused by the chloride ions from the NaCl content, premixed with the concrete. Also, other ions, such as sulfate, carbonate and bromide ions from the seawater and carbonate ions from the $NaHCO_3$ solution, were capable of breaking the protective passive film on the steel reinforcement. The passive film might have been stablized by the high concentration of hydroxyl ions associated with the concrete-pore electrolyte.

In the curves, it could be seen that the seawater was most corrosive, closely followed by the 1 M NaCl solution, then the 0.2 M $NaHCO_3$ solution, and the tap water the least corrosive throughout the whole experimental period. These results were not unexpected considering the chemical composition of the sea with its different, fairly high concentration of ions such as chloride, sulfate and carbonate ions. These ions have the capability of diffusing through the concrete matrix and depassivating the passive film at

[1] ICI, Lagos, Nigeria.

[2] Deutsches Institut fur Normung (DIN), Berlin, West Germany.

[3] Oshogbo Steel Rolling Mill, Oshogbo, Nigeria.

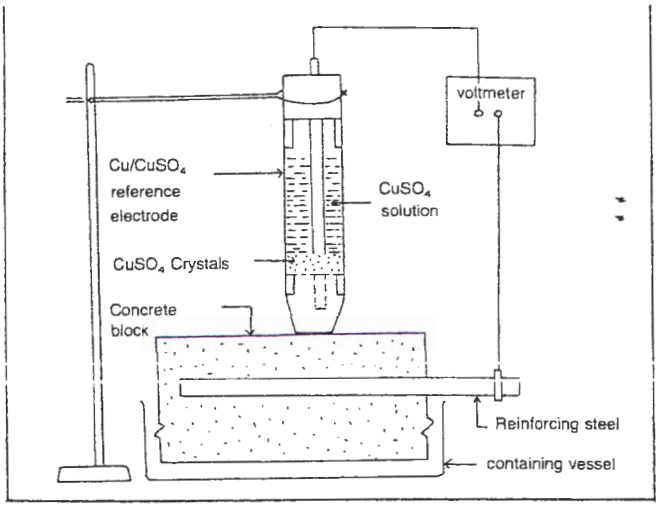

FIGURE 2. *Schematic diagram of the experimental set-up.*

the reinforced steel's surface. The NaCl solution also added more chloride ions to the already premixed quantities. The water from the solution and moisture from the atmosphere provided an adequate medium for the transport of the ions to the steel. The absorbed oxygen from the atmosphere diffusing through the concrete matrix and partially dissolving in the absorbed electrolytes would have aided the corrosion reactions of the steel in the concrete. The 0.2 M $NaHCO_3$ solution was less corrosive. This might be that the carbonate ions, $CO_3^{=}$, are less aggressive in corrosion reactions when compared with the chloride ions. In addition, the concentration of 0.2 M $NaHCO_3$ solution was low compared with 1 M NaCl. Nevertheless, the combination of the carbonate ions and the chloride ions from the premixed NaCl in the concrete would have caused further corrosion reactions with the potential achieving -400 mV_{CSE} on the 50th day.

Though the tap water curve indicated an active corrosion phenomenon and possibly anodic dissolution reactions at the steel/concrete interface, the corrosion reaction here was the lowest. The absorbed water and the chloride ions from the premixed NaCl content might have caused the active corrosion reactions leading to the increasing negative potential throughout the experimental period.

Effects of Coating the Reinforcement Steel

Figure 4 shows the relationship between the average corrosion potential and exposure time (days) for the steel-reinforced concrete blocks partially immersed in seawater, 0.2 M $NaHCO_3$ solution, 1 M NaCl solution, and tap water. The coating of the steel reinforcement here was designed to be a protective measure against the corrosion of the embedded steel.

Here also, the corrosion reactions trend was that of active corrosion with the negative potential increasing with time (after about the 10th day). This feature is more striking in the curves for the tests in seawater and 1 M NaCl solution. Some potential fluctuations could also be observed in the two curves (Figure 4). This probably suggests the occurrence of unstable repassivation phenomenon at the steel's surface. The curve for the test in seawater indicates more active corrosion and is closely followed (after 25 days of test) by that of the 1 M NaCl solution. The tap water shows the least tendency towards active corrosion.

Despite the observed phenomena of active corrosion reactions, anodic dissolution of the embedded steel's surface for the partially immersed samples in seawater and in 1 M NaCl solution appeared to have started after the 30th day of the test samples' immersion as indicated by the potential values. A potential of -200 to -350 mV_{CSE} indicates active or passive condition while -350 mV_{CSE} indicates active corrosion condition.[13] As on the 50th

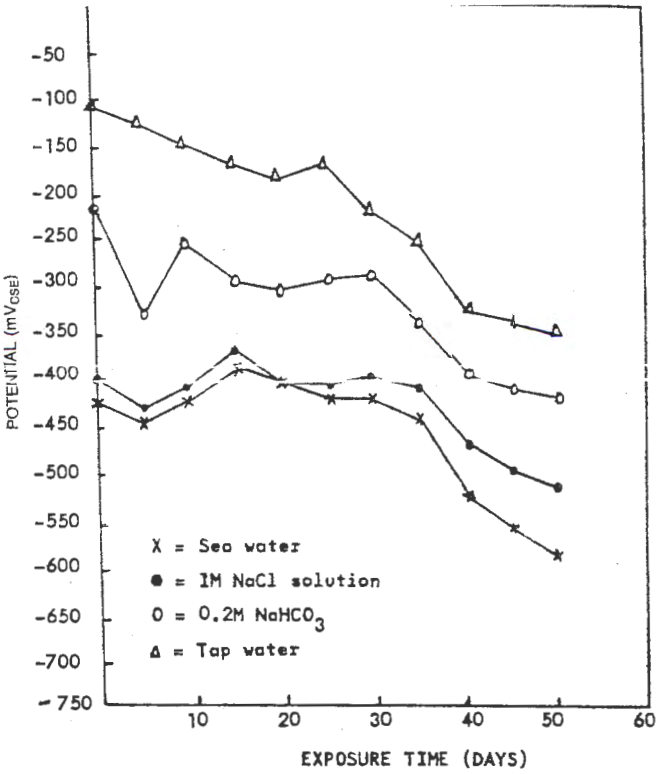

FIGURE 3. *Potential/exposure time curves for the mild steel-reinforced concrete (with NaCl) partially immersed in the different test environments.*

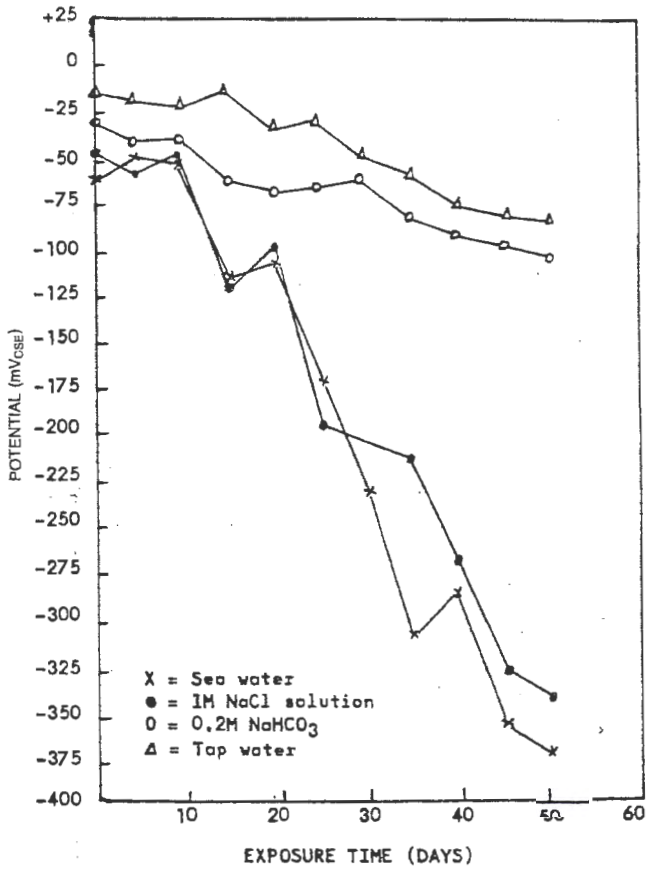

FIGURE 4. *Potential/time curve for mild steel(coated)-reinforced concrete block (without NaCl) partially immersed in the test environments.*

day, the corrosion of the steel reinforcement could not yet be described as intense. There were no forms of active dissolution at all for the test samples immersed in both the 0.2 M $NaHCO_3$ solution and the tap water throughout the whole experimental period, as indicated by the curves' potentials. These results and observations were not unexpected, however, since the coat of paint was meant to protect the steel reinforcement from getting in contact with reacting species, such as chloride, sulfate, and carbonate ions of the test media.

The sharply increasing negative potentials with time observed in the curves for the seawater and 1 M NaCl solution indicated active corrosion/interfacial chemical reactions. The coating was not fully protective until the end of the experimental period (the 50th day). This could not be unconnected with some defects in the paint coating, pinholes and scratches, that would have provided an access for the penetration of the reacting ions already absorbed into the concrete matrix and transported to the steel's surface by diffusion process for corrosion reactions.

The low concentration of the carbonate ions in the 0.2 M $NaHCO_3$ solution, and hence their probable inability to penetrate the coated surface of the steel or react with the paint, could contribute to the very near-passive nature of the test environment, as indicated by the curve in Figure 4. The chloride ion content of the tap water might be too insignificant to enable them to penetrate the steel's coating or react with it within the experimental period to cause its corrosion.

Effects of Coating the Concrete Blocks Externally with Paint

Figure 5 shows the effects of coating the concrete blocks externally with paint. The curves show increasing negative potentials with time. This indicates an active corrosion reaction. However, the recorded potentials as given in the curves could not be described as indicating corrosion by anodic dissolution. The results obtained as indicated in Figure 5 suggest that the embedded steel was protected throughout the experimental period[13] for all the test samples in the test media.

The tendency towards active corrosion was more pronounced, as indicated in the curves for the seawater and the 1 M NaCl solution and followed the trend previously described. Coating the concrete blocks externally (though leaving some portions on the top uncoated for the reference electrode contact) did not permit the test media to be absorbed into the concrete matrix and hence the reacting ion species from diffusing to the embedded steel surface for effective corrosion reactions. At the same time, the exposed top portions of the concrete block could allow the absorption of moisture and oxygen from the atmosphere to cause some corrosion reactions to occur at the steel/concrete interface, after some period of time. Nevertheless, the results given in Figure 5 suggest that anodic dissolution of the steel in concrete did not occur throughout the experimental period since the potentials remained in the range that could be considered to be outside the pitting or general corrosion potentials.

An observation of the concrete block at the immersed portion after the experimental period (50th day) showed some paint stripping. The stripping could allow the absorption of the test media into the concrete matrix at a very low rate. This might have been responsible for the differences observed in the active corrosion reactions as indicated in the curves. This possible assertion could be reasonably justified since some chloride ions from the seawater and NaCl solution and CO_3^{-2} ions from the $NaHCO_3$ solution could have diffused to the steel/concrete interface for corrosion reaction processes to occur.

The coated blocks, in general, are not meant to be continuously used in immersed conditions in liquid/aqueous environments, but in atmospheric environments. Therefore, the amount of protection given to the embedded steel under the test conditions and period in this investigation, as revealed in the curves (Figure 5), could be described as reasonably adequate.

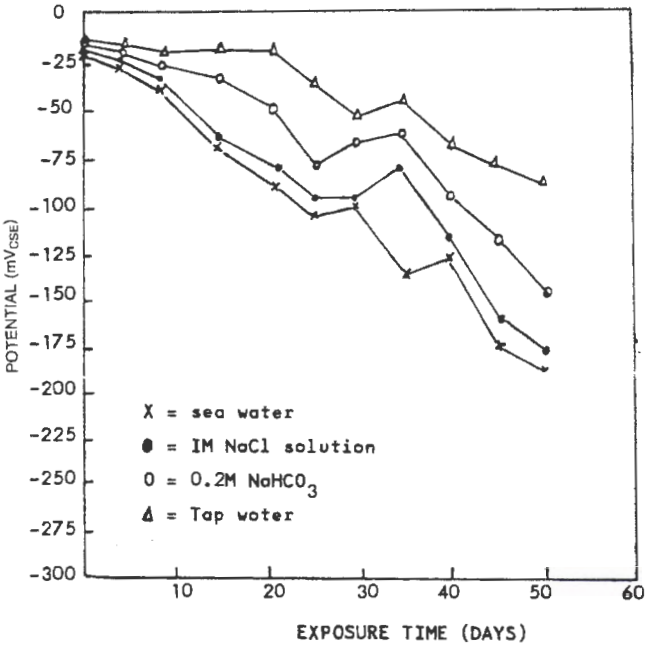

FIGURE 5. *Potential/exposure time curves for the steel-reinforced concrete blocks (without NaCl) coated externally and partially immersed in the test environments.*

Effects of Coating Both the Embedded Steel and the Concrete Blocks

Coatings of both the reinforcement steel and the concrete blocks offered very effective corrosion protection throughout the duration of the experiments. This was so in each of the test media in which the test samples were partially immersed. The potential changes observed in Figure 6 could be attributed to the effect of absorbed moisture and oxygen through the uncoated top part of the concrete blocks.

At the end of the 50th day of the experiments, some minor paint stripping was observed at the immersed parts of the blocks; it had no corrosive effect on the embedded steel. The results obtained here were not unexpected for these combined protective measures for the duration of this work, considering the individual protective ability of coating the embedded steel and the concrete blocks externally.

Statistical Analysis of Data

An insight into the mechanism of corrosion behavior of the embedded steel in concrete is further provided by analysis of some of the data (mean potential values) obtained; using the *least square method* (LSM) as shown in Figures 7 and 8. The results show a continuous increase of negative potentials with time, the relationship being negatively linear. This seems to be an indication of predominantly active corrosion reaction processes. It also indicates the possible occurrence of anodic dissolution of the embedded steel in concrete, resulting from the corrosion reaction processes at the steel/concrete interface. As expected, Figures 7 and 8 bear a close correlation to the corrosion trend previously discussed in Figures 3 and 4.

CONCLUSIONS

▶ Corrosion in mild steel-reinforced concrete is more severe in environments that consist of a combination of reacting ions, such as chloride, sulfate, and carbonate ions obtained in seawater.

▶ Coating of the embedded steel in concrete gives a considerable

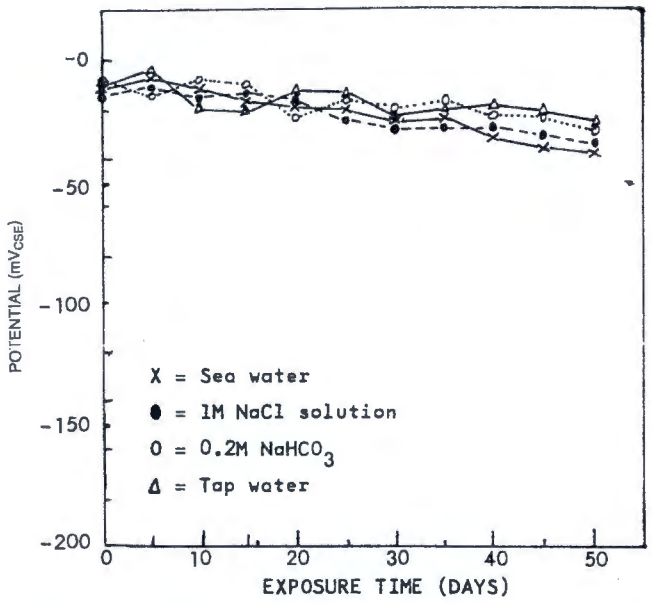

FIGURE 6. *Potential/exposure time curves for the coated steel-reinforced concrete blocks (both the embedded steel and the concrete blocks coated with paint) partially immersed in the different test media.*

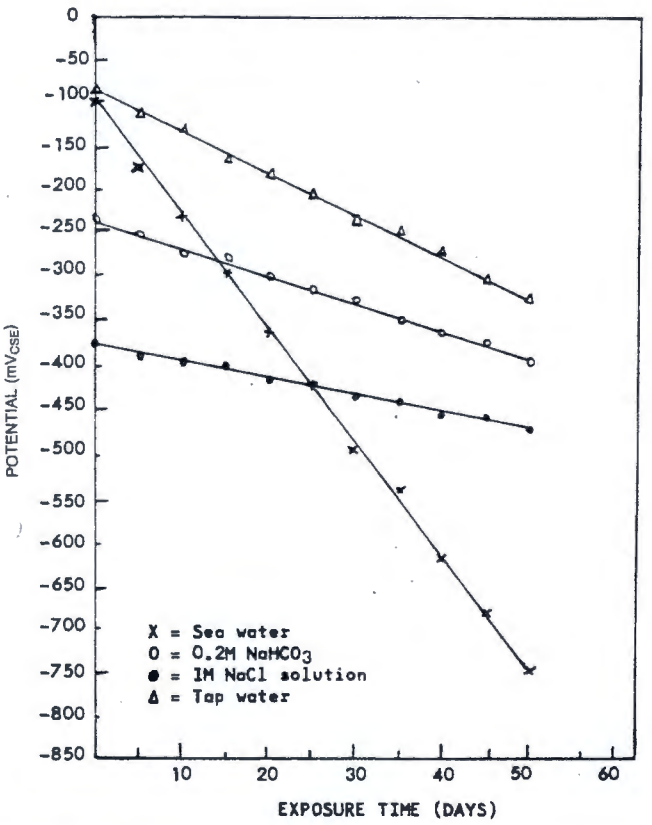

FIGURE 7. *Potential/time relationship (least square method) based on the data of Figure 3.*

measure of corrosion protection. Coating the blocks externally does not serve only the aesthetic purpose, but can give very good corrosion protection to the steel-reinforced concrete structures. A

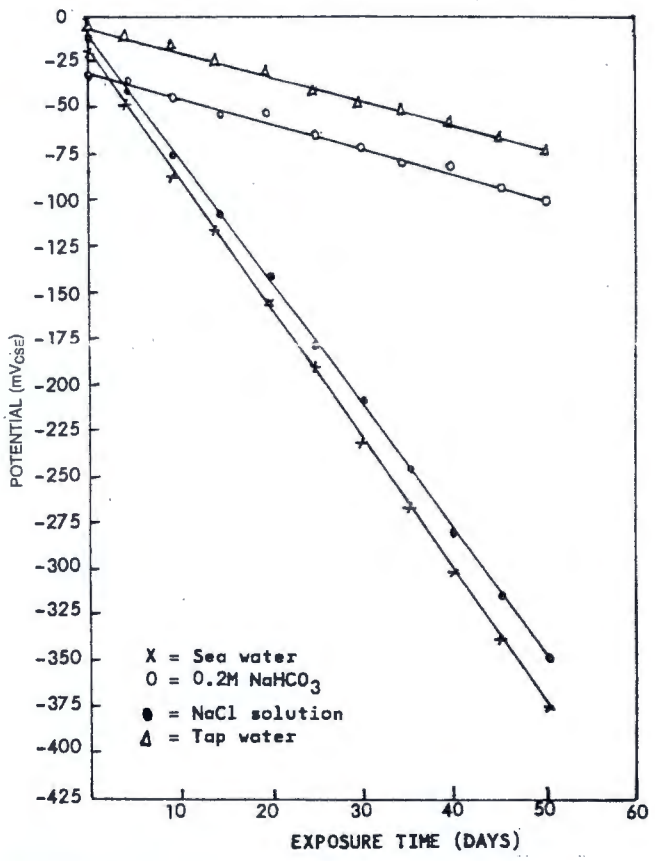

FIGURE 8. *Relationship of potential/time based on the least square method for the data of Figure 4.*

combination of the steel coating and the blocks (externally) gives the best protective measure, though the initial cost could be high.

▶ The overall corrosion behavior of the embedded steel in concrete shows that corrosion occurred by active dissolution of the reinforced steel. An insight into this mechanism is further provided by the statistical analysis of some of the data obtained.

ACKNOWLEDGEMENT

The authors are grateful for the provision of research facilities for this investigation from the Department of Metallurgical and Materials Engineering, Obafemi Awolowo University, Ile-Ife, Nigeria.

REFERENCES

1. "The Corrosion of Steel, and Its Monitoring, in Concrete," in Guides to Practice Series, Part 1 (London, UK: The Department of Industry, n.d.).
2. John E. Slater (Principal Investigator), Corrosion of Metals in Association with Concrete, Part 1, ASTM STP 818 (Philadelphia, PA: ASTM, 1983).
3. L. Page and J. Havdahl, Materials and Structures 18,103(1985): pp. 41-47.
4. R.T. Foley, Corrosion 26(1970): p. 58.
5. D.A. Hausmann, Materials Protection 15(1976): p. 19.
6. R.F. Stratfull, Corrosion 13(1957): p. 173t.
7. C.L. Page, Nature 258(1975): p. 514 .
8. D.A. Lewis and W.J. Copenhagen, Corrosion 15(1959): p. 382t.
9. V.K. Gouda and H.M. Mourad, Corrosion Science 14(1974): p. 687.
10. J.V. Sharp, Journal of Materials Science 14(1979): p. 1773.
11. R.L. Miller, W.H. Hartt and R.P. Brown, Materials Performance 15,5(1976): p. 20.
12. B.W. Cherry, Nga Ouack, and F.D. Beresford, Corrosion Australasia ,10(1983): p. 9.
13. ANSI/ASTM C876-77 Publication (Philadelphia, PA: ASTM, 1977), in Guides to Practice Series, Part 1 (London, UK: The Department of Industry, n.d.), p. 3.

Canadian Metallurgical Quarterly, Vol. 28. No. 3, pp. 259–263, 1989
Printed in Great Britain

0008–4433/89 $3.00 + .00

THE EFFECT OF COMPACTING PRESSURE AND SINTERING TEMPERATURE ON THE MECHANICAL AND PHYSICAL PROPERTIES OF SINTERED IRON POWDER PRE-PLATED WITH ELECTROLESS NICKEL

C. A. LOTO

Department of Metallurgical and Materials Engineering, Obafemi Awolowo University, Ile-Ife, Nigeria

(*Received* 17 *December* 1987; *in revised form* 15 *December* 1988)

Abstract—An investigation of the effect of compacting pressure and sintering temperature on the mechanical and physical properties of sintered iron powder pre-plated with electroless nickel was made using four different fractions of the powder and a dilute solution of commercial nickel sulphamate at a pH of 4.8 and a temperature of 90°C. The results obtained with varied compacting pressures and sintering temperatures for the mechanical and physical properties of the sintered products, suggest that a good homogeneity was obtained. There was an increase in elongation and a shrinkage in the thickness of the sintered compacts. Sintered strength and density increase with the growth in compacting pressure and in nickel content. Also, a considerable increase in sintered strength and elongation was obtained with the growth in sintering temperature.

INTRODUCTION

The effect of particle size distribution on the mechanical and physical properties of the sintered products of electroless nickel plated iron powders was demonstrated in recent work [1]. This article extends this by looking into the effects of compacting pressure and sintering temperature on the mechanical/physical properties of the sintered products resulting from the electroless nickel plating of iron powder fractions. A few data (Table 1 and Figs 7 and 8) from the previous work [1] are used here because of the significance of the results obtained and for discussion purposes. The relationships of the percentage elongation-to-fracture and dimensional changes, to both the compacting pressure and sintering temperature are separately examined in this case.

Various works have been done on electroless nickel plating [2–5]. The consequential heterogeneity in the materials microstructure which results in inferior mechanical properties due to the conventional elemental powder mixing/blending method has also been mentioned [6, 7].

While the previous work [1] has confirmed the feasibility of electroless nickel coating of iron powders by mechanical stirring technique, this work aims at making a further contribution to the characteristic mechanical/physical properties of the sintered products which were not studied in the earlier work.

Table 1. Coating thickness of the powder particles

Specimen	Average thickness (μm)
100 mesh	4.03
150 mesh	4.04
200 mesh	4.03
325 mesh	4.05

EXPERIMENTAL PROCEDURES

Plating process

The experimental procedures used here are described in the previous work [1]. The Hogannas iron powder ASC 100.29 (2.5 kg) was sieved into four different fractions using 100, 150, 200 and 325 mesh sieve. One litre of the diluted commercial nickel sulphamate solution which consists of nickel sulphamate of concentration 500 ml/l, boric acid 30 g/l and nickel chloride 5 g/l, was used for the plating of the iron powder fractions. The plating operation was carried out at a pH of 4.8 and a temperature of 90°C. The nickel plating solution was poured into a plating beaker and the beaker put into the plating bath. The surface of the solution in the bath was covered with chroffles to prevent excessive evaporation. A mechanical stirrer was used to bring the iron particles into suspension in the solution. Several platings of one hour each were made for each different fraction of the iron powder.

The coated iron powder after being washed several times with distilled water and with methanol, was dried in an electric oven set at a temperature of 120°C in air atmosphere. The coated powder was tested for nickel using dimethyl glyoxime dissolved in methanol. A purple colour precipitate showed the presence of nickel.

Specimen preparation

Green and sintered tensile specimens were made from the coated powders using tensile specimen dies of 6.45 cm^2 of surface area. A Deninson hydraulic press was used to make com-

pacts of 386, 541 and 695 MNm^{-2} pressure for each of the four different powder particle size ranges. A zinc stearate suspension was used as lubricant on the die walls to reduce the effect of friction and for easy removal of compacts from the die.

Sintering

The compacted specimens were sintered at temperature of 1120, 1080 and 1050°C using an atmosphere of cracked ammonia at 2.27 m^3/h and a furnace conveyor speed of 3.81 cm/min. The sintering time was 1 h. The sintered compacts were allowed to cool before removal from the furnace.

Determination of properties

The green and sintered densities of the samples were calculated after determining the volume and the mass of the samples.

The green and sintered strength of the samples were determined using an Instron tensometer. The strength of the samples was determined from the relationship

$$\text{Maximum stress} = \text{load/area}.$$

The percentage elongation of the samples was determined by bringing together the broken specimen and measuring the gauge length again. The percentage elongation for each of the samples was calculated as:

$$\%E = \frac{l_f - l_0}{l_0} \times 100$$

where $\%E$ = percentage elongation,
l_f = final length,
l_0 = original length.

The dimensional changes determination was made by using the vernier calipers to measure the sample length and a micrometer screw gauge to measure the width and thickness of the samples before and after sintering. The percentage shrinkage was determined as:

$$\%Sh = \frac{D_0 - D_f}{D_0} \times 100$$

where D_0 = original dimension,
D_f = final dimension,
$\%Sh$ = percentage shrinkage.

Microstructural examination was carried out on the mounted, polished and etched (2% Nital solution) as sintered specimens using an optical and the scanning electron microscopes.

The percentage nickel content of the compacts was determined using the S.E.M. by analysing the bulk mounted sample.

A micrometer eye piece was used with the optical microscope to determine the coating thickness of coated powder particles after mounting, grinding, polishing and etching with 2% Nital solution.

RESULTS AND DISCUSSION

Electroless nickel plating

The chemical test of dimethyl glyoxime for nickel and the metallographic examination with optical microscope confirmed the possibility of coating iron powder with nickel by means of the electroless plating method used. The deposit was found to be uniform (within the limit of any experimental error) in thickness as given in Table 1, regardless of the size or shape of the coated surface.

As previously reported [1], the iron powder particles used provided a large surface area for chemical reaction and hence whenever powder was poured in, there was effervescence caused by an evolution of hydrogen gas and with the formation of foam. It was also observed all the time that the nickel plating solution lost its greenish colour substantially after the first few minutes of plating. This might be an indication that the reaction was faster within the first 15 min than during the rest of the plating time.

The coated powder produced at the end of the coating did not show any appreciable change in colour; it became dull and when dried in an oven part of it became slightly oxidised. This means that electroless nickel coating of iron powder did not prevent the oxidation of the powder particles, due to the introduction of some quantities of oxide impurity.

The effect of compacting pressure

The curves showing the effect of compacting pressure on green density of the pre-plated iron powder have previously been indicated as Fig. 1 in [1]. The positive slopes show that the green density increases with increasing compacting pressure for all the powder particle size ranges used. This increase in green compact density with increasing compacting pressure might be due to the increased plastic deformation and the fracture of individual particles which might have enhanced more particle-to-particle contact and densification. Increase in

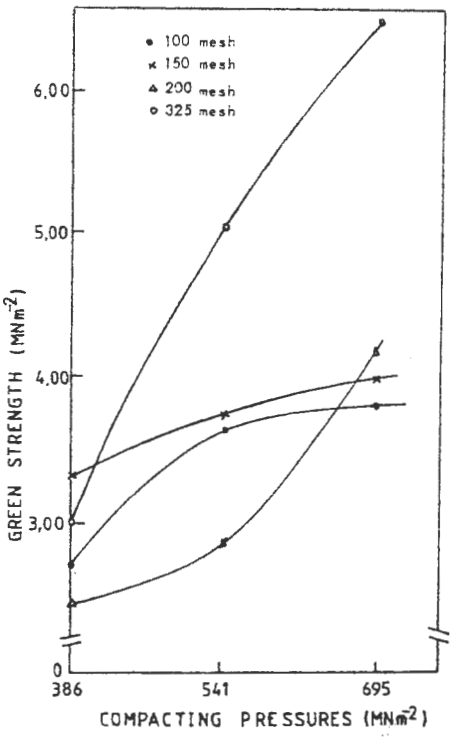

Fig. 1. The effect of compacting pressure on green strength.

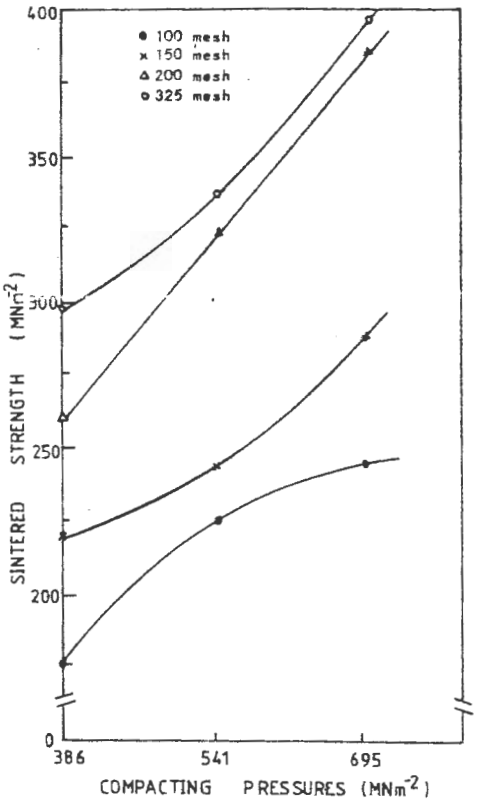

Fig. 2. The effect of compacting pressure on sintered strength. Sintering temperature: 1120°C.

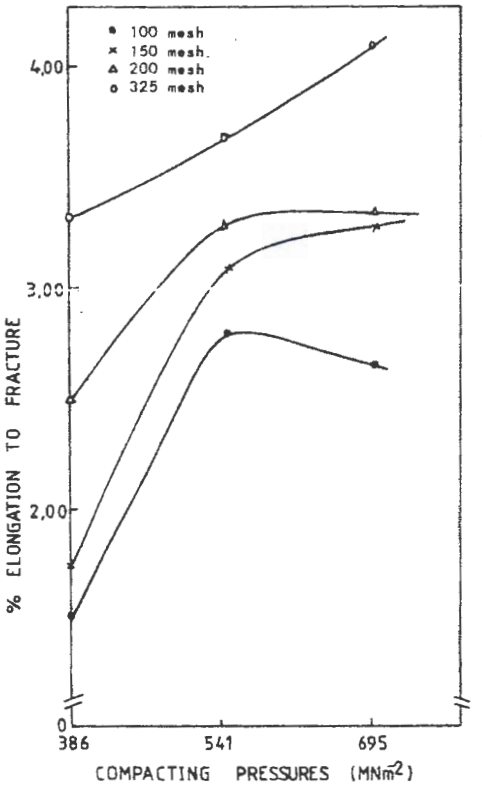

Fig. 3. The effect of compacting pressure on elongation. Sintering temperature: 1120°C.

compacting pressure could also lead to increased particle movement which promotes densification.

It is also observed that sintered density increases with increase of compacting pressure for all four different powder fractions used. This observation has previously been indicated [1] with respect to the effect of particle size distribution. Plastic deformation produced by increasing compacting pressure gives increased stresses and this might provide greater interparticle contact for volume diffusion paths. A probable inference then is that the greater the compacting pressure, the more the stresses produced and the more the transport of vacancies and atoms during sintering which enhances more densification.

Figure 1 shows that the green strength increases with increasing compacting pressure. This phenomenon might have resulted chiefly from mechanical interlocking of the irregularities on the particle surfaces as a result of increasing compacting pressure.

Figure 2 shows that sintered strength increases with increase in compacting pressure for all the coated iron powder fractions. This could be due to the fact that increase in compacting pressure creates increasing plastic deformation. Plastic deformation creates large interparticle contact areas which grow by diffusional mass transport during sintering and thus confers strength.

There is increase in elongation with increasing compacting pressure except for the 100 mesh test specimens which reaches its maximum elongation at a compacting pressure of 541 MNm^{-2}. This behaviour of the 100 mesh material is difficult to explain. However, it may not be unconnected with the loss of ductility at higher compacting pressure due to increased dislocation density created by plastic deformation which could not be relieved by sintering at the temperature used (Fig. 3). With lower porosity of the compacts due to the increasing compacting pressure, bulk movement of particles of the compact will be enhanced. There will also be plastic deformation and fracture of particles. These could promote densification which may result into higher sintering, more strength and elongation.

A decrease in shrinkage in the thickness of the sintered compacts with increasing compacting pressure is observed (Fig. 4). This phenomenon may be explained by the increasing compacting pressure which might have closed the pores. The closure of the pores may result in higher green density which leads to smaller rate of densification during the sintering treatment and hence the smaller value of dimensional change.

The effect of sintering temperature

The parameters investigated here are elongation, linear shrinkage behaviour, sintered density and strength.

There is an increase in elongation with increase in sintering temperature for all particles size ranges (Fig. 5). The 325 mesh powder falls out of the trend of 100 mesh > 150 > 200 > 325 mesh. Though this type of observation had been reported [8], the trend in this investigation might be due to nickel content effect. The 325 mesh powder being the finest powder, and thus having larger surface area, has more nickel content percentage (3.70%). This seems to have increased its tensile strength and ductility. The effect is more noticeable at very high temperature (1120°C) where the nickel diffusion into the iron matrix to form

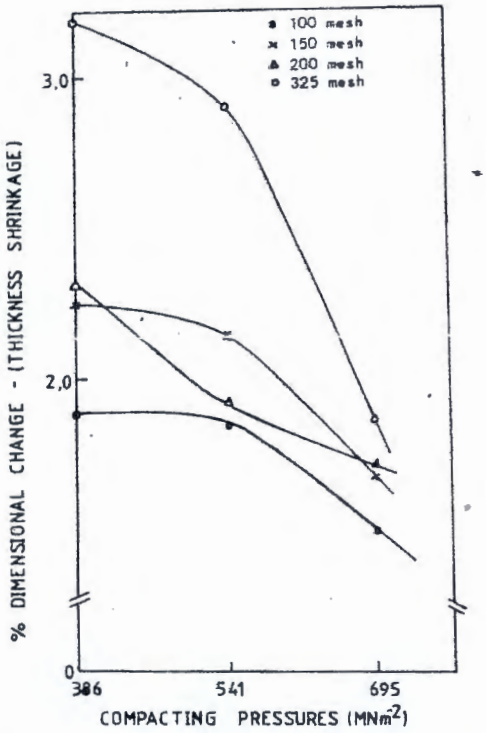

Fig. 4. The effect of compacting pressure on the linear shrinkage behaviour of the sintered compacts. Sintering temperature: 1120°C.

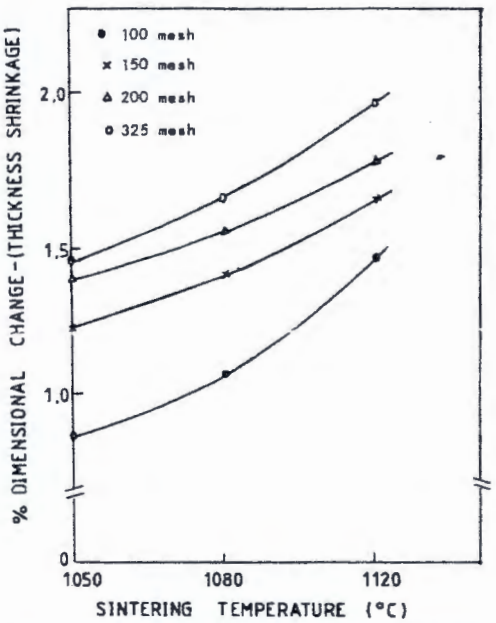

Fig. 6. The effect of sintering temperature on the linear shrinkage behaviour of the sintered compacts. Compacting pressure: 695 MNm^{-2}.

homogeneous solution is higher as indicated in Fig. 5. It has been established by various other workers that temperature causes increased pore-rounding and shrinkage. These effects increase with increasing sintering temperature. Since shrinkage reduces the amount of porosity by the closing and rounding of pores as a result of particle diffusion, it is expected that fracture will be reduced thus enhancing ductility. With increased temperature, there would be more atomic mobility, increase in rate of diffusion and mass movement due to heat energy of molecular and atomic vibration. These phenomena could

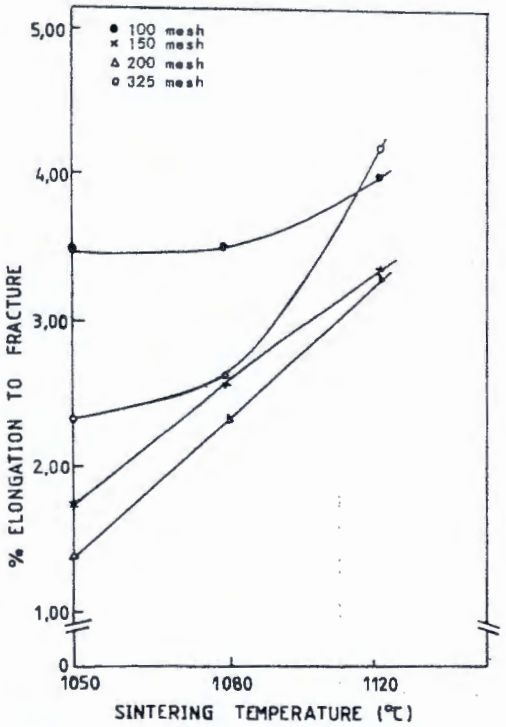

Fig. 5. The effect of sintering temperature on elongation. Compacting pressure: 695 MNm^{-2}.

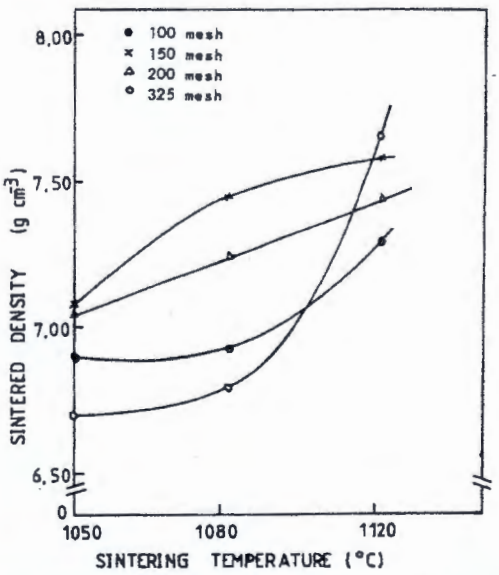

Fig. 7. The effect of sintering temperature on sintered density. Compacting pressure: 695 MNm^{-2}.

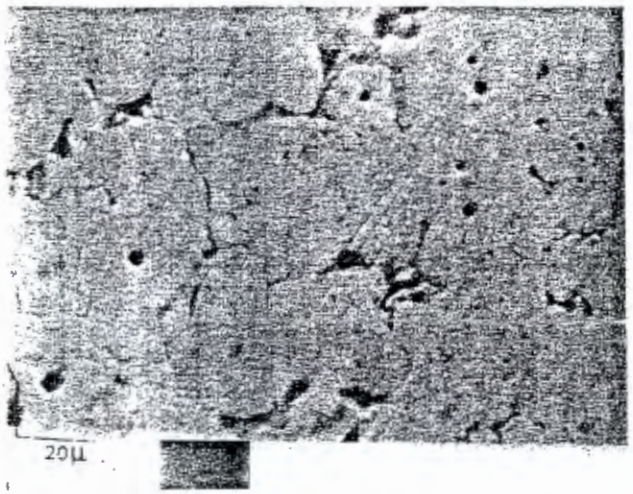

Fig. 8a. 200 mesh sintered compact at 695 MNm^{-2} sintering temperature at 1120°C. Etched in 2% Nital reagent.

Fig. 8b. 325 mesh sintered compact at 695 MNm^{-2} sintering temperature at 1120°C. Etched in 2% Nital reagent.

enhance better sintering with better mechanical properties of tensile strength and elongation.

An increase in shrinkage of the sintered compacts with increasing temperature (Fig. 6) is observed. This phenomenon may be understood from the fact that an increase in sintering temperature causes increase in surface diffusion, volume diffusion, grain boundary diffusion and plastic flow. The increasing mobility of atoms of the material and material transport during sintering of the compacts could result in bonding between the powder particles at an earlier stage. It could also result in shrinkage and densification at a later stage. It can therefore be inferred that the higher the temperature, the more readily the above material transport mechanisms occur and the greater is the densification and shrinkage as observed in the sintered compacts under investigation. While sintering continues at higher temperatures, there seems to be a steady decrease in porosity. However, since this might be impossible without simultaneous material movement into the voids, it follows that the continuation of sintering might cause a corresponding decrease in over-all volume and linear shrinkages in the various directions of the compact.

Figure 7 shows that for all ranges of particle size in this investigation, the sintered density increases with increasing sintering temperature [1]. The reasons for this phenomenon have been discussed above. Nevertheless, densification could be enhanced by increased temperature. This might be due to the greater material transport created within the compact because of increased atomic mobility resulting from high and increasing temperature. Bonding is therefore promoted and a decrease in porosity is enhanced (Figs 8a,b). This explanation accounts for the different behaviour of the 325 mesh material at 1120°C. The material has the finest particles and hence greater surface area for interparticle contact. This provides for easier diffusion more particularly at higher temperatures and thus increased densification.

The effect of sintering temperature on sintered strength with respect to particle size distribution has been shown in an earlier study [1]. The sintered strength increased with increasing sintering temperature for all ranges of particle size. This increase of sintered strength seems to be due to the increasing temperature which enhances greater transport of materials for bonding, diffusion of particles and densification with the closing and rounding of pores.

CONCLUSIONS

(1) With increase in compacting pressure, there is an improvement in mechanical and physical properties for pre-plated iron powders with respect to green density and strength, sintered density and strength, elongation and linear shrinkage behaviour. The powder fractions of 325 mesh sieve show the best properties in most cases.

(2) Sintered density and sintered strength increase with increase of temperature.

(3) The improved mechanical and physical properties obtained for the sintered iron powder (Ni-pre-plated) in this work suggests that a good homogeneity of diffused nickel in iron matrix is achieved.

REFERENCES

1. C. A. Loto, *J. Metals* **39**(8), 36 (1987).
2. L. F. Spencer, *Metal Finishing* **72**, 58–64 (1974).
3. R. M. Burns and W. M. Bradley, *Protective Coatings for Metals*, pp. 229–230. Reinhold (1974).
4. A. Brenner and G. E. Riddell, *Proc. Am. Electropl. Soc.* **34**, 156–179 (1947).
5. W. Canning, *The Canning Handbook on Electroplating*, 20th Edn, pp. 245–429 (1978).
6. P. Lindskog and G. Skoglund, *3rd Eur. P/M Symp. Conf.*, Suppl. pt I, p. 375 (1971).
7. H. Dixon, A. J. F. Fletcher and R. T. Cundill, *Power Metall.* **21**(3), 131 (1978).
8. P. Schwarzkopf, *Powder Metallurgy: Its Physics and Production*, p. 82. Macmillan, New York (1947).